The copper chaperone CCS facilitates copper binding to MEK1/2 to promote kinase activation

JBC RESEARCH ARTICLE

The copper chaperone CCS facilitates copper binding to MEK1/2 to promote kinase activation

Received for publication, March 30, 2021, and in revised form, October 12, 2021 Published, Papers in Press, October 27, 2021,
https://doi.org/10.1016/j.jbc.2021.101314

Michael Grasso[1,2], Gavin J. Bond[2,3,4,‡], Ye-Jin Kim[2,4,‡], Stefanie Boyd[5], Maria Matson Dzebo[6], Sebastian Valenzuela[6], Tiffany Tsang[2,4,7], Natalie A. Schibrowsky[1,2], Katherine B. Alwan[8], Ninian J. Blackburn[8], George M. Burslem[4,9], Pernilla Wittung-Stafshede[6], Duane D. Winkler[5], Ronen Marmorstein[1,2,9], and Donita C. Brady[2,4,*]

From the [1]Department of Chemistry, School of Arts and Sciences, [2]Abramson Family Cancer Research Institute, Perelman School of Medicine, [3]Biochemistry Major Program, College of Arts and Sciences, and [4]Department of Cancer Biology, Perelman School of Medicine, University of Pennsylvania, Philadelphia, Pennsylvania, USA; [5]Department of Biological Sciences, University of Texas at Dallas, Richardson, Texas, USA; [6]Department of Biology and Biological Engineering, Chalmers University of Technology, Gothenburg, Sweden; [7]Cell and Molecular Biology Graduate Group, Perelman School of Medicine, University of Pennsylvania, Philadelphia, Pennsylvania, USA; [8]Department of Chemical Physiology and Biochemistry, School of Medicine, Oregon Health and Science University, Portland, Oregon, USA; [9]Department of Biochemistry and Molecular Biophysics, Perelman School of Medicine, University of Pennsylvania, Philadelphia, Pennsylvania, USA

Edited by Alex Toker

Normal physiology relies on the precise coordination of intracellular signaling pathways that respond to nutrient availability to balance cell growth and cell death. The canonical mitogen-activated protein kinase pathway consists of the RAF-MEK-ERK signaling cascade and represents one of the most well-defined axes within eukaryotic cells to promote cell proliferation, which underscores its frequent mutational activation in human cancers. Our recent studies illuminated a function for the redox-active micronutrient copper (Cu) as an intracellular mediator of signaling by connecting Cu to the amplitude of mitogen-activated protein kinase signaling *via* a direct interaction between Cu and the kinases MEK1 and MEK2. Given the large quantities of molecules such as glutathione and metallothionein that limit cellular toxicity from free Cu ions, evolutionarily conserved Cu chaperones facilitate efficient delivery of Cu to cuproenzymes. Thus, a dedicated cellular delivery mechanism of Cu to MEK1/2 likely exists. Using surface plasmon resonance and proximity-dependent biotin ligase studies, we report here that the Cu chaperone for superoxide dismutase (CCS) selectively bound to and facilitated Cu transfer to MEK1. Mutants of CCS that disrupt Cu(I) acquisition and exchange or a CCS small-molecule inhibitor were used and resulted in reduced Cu-stimulated MEK1 kinase activity. Our findings indicate that the Cu chaperone CCS provides fidelity within a complex biological system to achieve appropriate installation of Cu within the MEK1 kinase active site that in turn modulates kinase activity and supports the development of novel MEK1/2 inhibitors that target the Cu structural interface or blunt dedicated Cu delivery mechanisms *via* CCS.

The development of a multicellular organism depends on the precise synchronization of cell division, death, specialization, interactions, and movement. The orchestration of complex cellular processes in response to environmental changes is essential for organismal tissue homeostasis. Intrinsic molecular mechanisms enable the conversion of fluctuating extracellular and intracellular inputs into various outputs that drive cellular processes necessary for adaptation (1, 2). This interpretation and integration of inputs is controlled by signal transduction pathways that facilitate the precise coordination of cellular processes with dynamic spatial and temporal control (1, 2). One of the simplest evolutionarily conserved mediators of signal transduction is the protein kinase, an enzyme that traditionally phosphorylates a substrate at threonine, serine, and/or tyrosine residues (3). Kinases within complex protein modules directly respond to and/or sense growth factors, nutrients, and metabolites to influence signal amplification, duration, and frequency (1, 2).

Although the kinase signaling networks that integrate fluctuations in the abundance of many nutrients and metabolites are well-established (1, 2), the discovery of signaling molecules capable of mediating similar functions downstream of transition metal availability is underdeveloped. Traditionally, the redox-active transition metal copper (Cu) functions as a high affinity structural and/or catalytic cofactor within the active site of Cu-dependent enzymes (4–6). Phenotypic studies of the rare genetic diseases, Menkes and Wilson, solidified the physiological impact of aberrant Cu absorption and excretion (7–10). Mechanistically, these diseases display deficiencies in cellular functions attributed to the dozens of known Cu-dependent enzymes and helped elucidate the cellular machinery responsible for the proper acquisition and distribution of Cu (5, 7, 8). Despite the need for strict homeostatic mechanisms to control Cu abundance, we know relatively little about direct kinase signaling pathways that respond to and or/

‡ These authors contributed equally to this work.
* For correspondence: Donita C. Brady, bradyd@pennmedicine.upenn.edu.

sense Cu abundance, especially those that integrate to influence cellular proliferation.

In pursuit of providing a molecular explanation for the observations that biological systems convert Cu abundance into cellular decisions like proliferation (11), we recently reported an unexpected link between the cellular acquisition of Cu and a mitogenic signaling cascade instrumental in cell proliferation (12). Namely, genetic ablation of the primary Cu transporter gene *Ctr1*, which in multiple organisms results in growth retardation and embryonic lethality (13–15), reduced mitogen-activated protein kinase (MAPK) signaling downstream of growth factor stimulated receptor tyrosine kinase activation (12). The canonical MAPK pathway consists of the RAF-MEK-ERK signaling cascade and represents one of the most well-defined axes within eukaryotic cells to promote cell proliferation (16). In response to receptor tyrosine kinase activation, GTP-bound rat sarcoma virus GTPase engages the serine/threonine rapidly accelerated fibrosarcoma protein kinases *via* their rat sarcoma virus binding domains to promote phosphorylation and activation of the MEK1 and MEK2 kinases, which in turn phosphorylate and activate the ERK1 and ERK2 kinases to drive cell proliferation (17, 18). Layered on top of this signaling cascade are the multiple positive and negative regulatory mechanisms that fine-tune the frequency, duration, localization, and amplitude of canonical MAPK signaling (19), underscoring the importance of tightly regulating this pathway at the cellular and organismal level for a host of responses. Genetic, molecular, and biochemical interrogation of the requirement of Cu for MAPK pathway activation revealed a direct metal-kinase interaction between Cu and MEK1/2 that was sufficient to augment phosphorylation and activation of the ERK1 and ERK2 kinases (12). This is the first example of Cu directly regulating the activity of a mammalian kinase and has exposed a signaling paradigm that directly connects Cu to the signaling pathway components (6). Further, targeting aberrant MAPK signaling in melanomas and other cancers (20–22) contributes to the efficacy of Cu chelators (23–26) that are traditionally used to treat Cu overload in Wilson disease patients (7) and highlights the importance of dissecting the molecular mechanism of MEK1/2 activation *via* Cu.

In the present study, we set out to interrogate the mechanism by which selective Cu delivery and subsequent MEK1/2 activation is achieved. *In vitro* and in mammalian cells, Cu-stimulated MEK1/2 kinase activity required the Cu chaperone for superoxide dismutase (CCS) and could be blocked with the small molecule inhibitor DCAC50 that targets CCS. Taken together, the data provide a more precise understanding of how Cu cooperates with MEK1/2 that can be used to expand the landscape of Cu in kinase signal transduction.

Results

CCS binds MEK1 to facilitate Cu binding and increased kinase activity

We first explored the existence of a dedicated cellular Cu delivery mechanism capable of supporting Cu-stimulated MEK1/2 activity. The evolutionarily conserved Cu chaperones facilitate the efficient delivery of Cu to cuproenzymes located in the cytosol, trans-Golgi network, or mitochondria (27). Based on the predominant cytosolic localization of MEK1/2, we tested whether the cytosolic Cu chaperones ATOX1 or CCS bind to MEK1 in single-cycle surface plasmon resonance (SPR) experiments. The recombinant MEK1 was coupled to a SPR sensor followed by injection of increasing concentrations of parvalbumin (Fig. 1*A*), as a negative control, or the Cu chaperones ATOX1 or CCS (Fig. 1, *B* and *C*). CCS interacted with MEK1 at an apparent dissociation constant (K_D) of 2.09 ± 0.48 μM (Fig. 1*C*; Table 1) when compared with ATOX1 (Kd = 10.9 ± 5.65 μM), confirming a direct interaction between CCS and MEK1. However, both electrophoretic mobility shift assay and size-exclusion chromatography (SEC) of excess MEK1 or CCS suggest that the association between apo-CCS or Cu-CCS and MEK1 is transient based on the absence of a stable complex that could be coeluted (Fig. 1, *D*–*G*).

We next interrogated the relationship between the Cu chaperones and MEK1 kinase activity and Cu binding *in vitro*. A selective 3-fold enhancement in MEK1 kinase activity was observed when increasing concentrations of Cu loaded CCS, but not ATOX1, were added to MEK1 kinase assays (Fig. 1*H*), indicating that CCS is directly involved in Cu-stimulated MEK1/2 phosphorylation of ERK1/2 (24). Based on the observation that CCS, which binds Cu(I), increased MEK1 kinase activity, we evaluated whether this increase in activity was driven by Cu transfer. Stoichiometric addition of Cu-CCS to MEK1 and subsequent separation by SEC to capture MEK1 positive fractions for analysis by inductively-coupled plasma mass spectrometry (ICP-MS) resulted in an average of 1.068 Cu atoms bound per MEK1 protomer, which is significantly above the as isolated MEK1 protein from bacteria (Fig. 1, *I* and *J*). As an important control, we next tested whether CCS transfer of Cu to MEK1 can occur in the presence of the Cu(I) chelator bathocuproinedisulfonic acid (BCS) and found an average increase of 0.95 Cu atoms bound per MEK1 protomer (Fig. 1, *I* and *J*), which suggests that CCS is acting as a bonafide Cu chaperone for MEK1 instead of MEK1 binding Cu in solution. Further, when compared with a control sample in which CCS was incubated with Cu to determine stoichiometry, we detected a reduction in CCS Cu binding from typical 1:1 to either 0.5 Cu atoms or 0.2 Cu atoms per protomer when incubated with MEK1 in either the presence or absence of BCS, respectively (Fig. 1, *I* and *J*). Taken together, these data support a scenario in which the cytosolic Cu chaperone CCS functions as a direct Cu delivery mechanism to MEK1 *via* a transient association that in turn facilitates increased kinase activity.

Cu integration into MAPK signaling requires CCS Cu binding

To directly address an association between CCS and MAPK signaling in mammalian cells, BirA proximity-dependent biotin identification (BioID) reagents were generated to capture the weak or transient interaction between ATOX1 or CCS with MEK1 in living cells. Specifically, myc-epitope tagged mutant (R118G) BirA biotin ligase, which conjugates biotin to

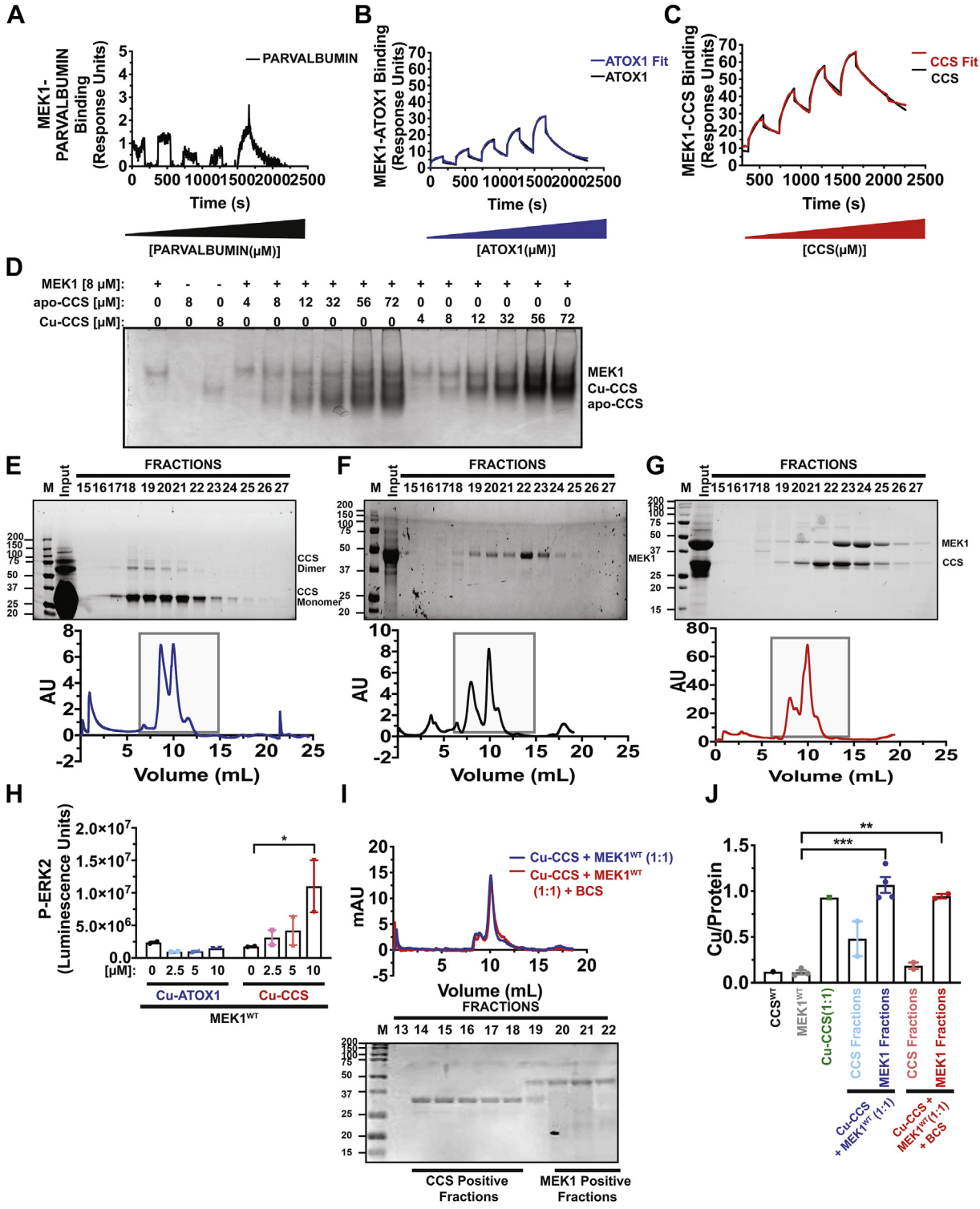

Figure 1. CCS directly interacts with MEK1 to facilitate Cu binding and kinase activity. *A–C*, single-cycle SPR experiments of HIS-tagged PARVALBUMIN, ATOX1, or CCS binding to MEK1 in which increasing concentrations of (*A*), PARAVALBUMIN (2.5–40 μM, *black line*), (*B*), ATOX1 (2.5–40 μM, *blue line*), or (*C*), CCS (5–40 μM, *red line* was injected onto immobilized MEK1 and the The 1:1 binding model fits [*B*] *black lines*). n = 3 independent experiments. *D*, electrophoretic mobility shift assays (EMSAs) of increasing concentrations of apo-CCS or Cu reconstituted CCS (Cu-CCS) with increasing concentrations of MEK1. *E–G*, size exclusion chromatography runs of (*E*), Cu-CCS (*blue line*), (*F*), MEK1 (*black line*), or (*G*), Cu-CCS and MEK1 (*red line*) and protein detection in indicated fractions detected by Coomassie Brilliant Blue. *H*, scatter dot plot with bar at mean luminescence units ±SEM from ELISA detection of recombinant phosphorylated (P)-ERK2^{K54R} from MEK1^{WT} incubated with increasing concentrations of Cu reconstituted ATOX1 (Cu-ATOX1) or CCS (Cu-CCS). n = 2 technical replicates. The results were compared using a two-way ANOVA followed by a Tukey's multi-comparisons test. *p = 0.0185. *I*, size exclusion chromatography runs of Cu-CCS and MEK1 mixed 1:1 (*blue line*) or Cu-CCS and MEK1 mixed 1:1 in presence of 5:1 ratio of bathocuproinedisulfonic acid (BCS) to protein (*red line*) and CCS or MEK1 positive fractions analyzed by inductively-coupled plasma mass spectrometry (ICP-MS) detected by Coomassie Brilliant Blue. *J*, scatter dot plot with bar at mean ratio of Cu detected by ICP-MS to protein ±SEM of CCS, as isolated, MEK1, as isolated, Cu and CCS mixed 1:1, CCS positive fractions 14 to 18 or MEK1 positive fractions 20 to 22 from Cu-CCS and MEK1 mixed 1:1, or CCS positive fractions 14 to 18 or MEK1 positive fractions 20 to 22 from Cu-CCS and MEK1 mixed 1:1 in presence of BCS. n = 1 to 4 independent experiments. The results were compared using one-way

Table 1
Association (k_a), dissociation rate constant (k_d), dissociation constant (K_d), and predicted maximum response (R_{max}) of ATOX1 or CCS binding to MEK1 obtained with SPR

Protein	k_a ($M^{-1}s^{-1}$)	k_d (s^{-1})	K_d (μM)	R_{max} (RU)
ATOX1	309 ± 109	(3.07 ± 0.55) × 10^{-3}	10.9 ± 5.65	28.67 ± 3.92
CCS	533 ± 163	(1.06 ± 0.12) × 10^{-3}	2.09 ± 0.48	67.39 ± 4.92

SPR data was fitted with a 1:1 binding model, and the presented values are the average and SD of mean (n = 3 independent experiments).
Abbreviation: k_a, association constant; k_d, dissociation rate constant; R_{max}, predicted maximum response.

proteins within the immediate vicinity (∼10 nm) (28), was fused in frame to the N-terminus of ATOX1 or CCS and stably expressed in HEK-HT cells (Fig. 2*A*). As expected, exogenous biotin treatment of HEK-HT cells expressing myc-BirA-ATOX1 resulted in the streptavidin recovery of biotinylated ATP7A (5, 27) (Fig. 2*A*), which facilitates the transport of Cu into the lumen of the trans-Golgi network where Cu loading of Cu-dependent enzymes occurs, whereas myc-BirA-CCS biotinylated SOD1 (5, 27, 29) (Fig. 2*A*) uses Cu as a cofactor for catalyzing the disproportionation of superoxide to hydrogen peroxide and dioxygen. Endogenous MEK1 was only biotinylated in presence of biotin and myc-BirA-CCS, indicating that CCS is proximal to MEK1/2 and may be responsible for Cu-stimulated activation of MAPK signaling. Interestingly, streptavidin recovery of biotinylated MEK1 from exogenous biotin treatment of HEK-HT cells expressing myc-BirA-CCS was significantly reduced in response to treatment with the Cu(I) chelator BCS and was unaffected by exogenous $CuCl_2$ (Fig. 2*B*).

To investigate whether CCS Cu binding is necessary for endogenous MAPK signaling, *CCS* was knocked down with two independent doxycycline-inducible shRNAs in HEK-HT cells. The knockdown of *CCS* decreased basal and either $CuCl_2$ or epidermal growth factor stimulated activation of P-ERK1/2 (Fig. 2, *C* and *D*). Given the well characterized contribution of CCS to SOD1 Cu binding, we tested whether the loss of CCS was primarily acting through a direct CCS-MEK1 interaction and not a parallel pathway in which SOD1 activity is reduced. In contrast to the knockdown of *CCS* (Fig. 2, *C* and *D*), we found that decreased expression of *SOD1* reduced both MEK1/2 and ERK1/2 phosphorylation (Fig. 2*E*). These data are in agreement with a previously proposed mechanism in which loss of SOD1 activity should reduce H_2O_2 and as a consequence, protect protein phosphatases from H_2O_2-mediated inactivation and promote dampened MAPK pathway activation (30). Thus, our data suggest that abrogated CCS function works *via* a differential mechanism that is specific to the level of MEK1/2 activity.

CCS-mediated metalation of SOD1 involves three distinct domains of CCS that are each required for SOD1 activity. Domain 1 (D1) facilitates Cu acquisition, domain 2 (D2) mimics SOD1 to promote protein-protein interactions, and domain 3 (D3) may be involved in D1 to D3 Cu transfer while also generating the disulfide bond necessary for SOD1 activation (27, 31, 32). To definitively test the contribution of CCS D1 and D3 to MAPK signaling, HEK-HT stably expressing nontargeting control or doxycycline-inducible *CCS* shRNA in the presence of exogenous WT or mutant CCS at the Cu binding interface of D1, D3, or both were generated (Fig. 2*F*). Based on its inability to acquire Cu regardless of the source, mutation of CCS D1 resulted in reduced P-ERK1/2 (Fig. 2*F*). Surprisingly, D3 of CCS was also required for basal P-ERK1/2 levels (Fig. 2*F*), suggesting that a similar mechanism by which CCS activates SOD1 may be used to facilitate Cu-dependent CCS-mediated activation of MEK1/2 (31, 32) and is supported by the combined D1/D3 mutant not exhibiting an exacerbated phenotype. Despite our expectations, the knockdown of *CCS*, which specifically resulted in reduced ERK1/2 phosphorylation (Fig. 2, *C* and *D*), had little to no effect on SOD1 function, as measured *via* in gel activity assays (Fig. S1*A*). Taken together, these results indicate that CCS is an integral component of MEK1/2 responsiveness to both Cu and growth factors.

Targeting CCS with the small molecule inhibitor DCAC50 reduces MEK1/2 activity

A recent study described the development and characterization of a small molecule inhibitor, DCAC50, targeting the Cu chaperones ATOX1 and CCS (33). Mechanistically, DCAC50 binds ATOX1 and CCS with K_D of 6.8 ± 1.7 μM and 8.2 ± 2.7 μM, respectively, and prevents Cu transfer between the chaperones and their downstream interacting target proteins (33). Thus, to investigate whether acute inhibition of CCS would decrease MAPK pathway activation in an analogous fashion to genetic deletion of *CCS* (Fig. 2, *B* and *C*), the HEK-HT cells were treated with increasing concentrations of DCAC50. Similar to loss of *CCS*, P-ERK1/2 was reduced in response to DCAC50 treatment in a dose-dependent fashion (Fig. 3*A*). In agreement with our findings that genetic ablation of *CCS* has little impact on SOD1 function, we similarly observed no change in SOD1 activity in the HEK-HT cells treated with increasing concentrations of DCAC50 (Fig. S1*B*). Further, the kinetics of MAPK pathway activation by $CuCl_2$ or epidermal growth factor were dampened and delayed in the presence of DCAC50 (Fig. 3, *B* and *C*). These results support our findings that CCS is directly required for MAPK signaling by contributing to MEK1/2 Cu binding and suggest another avenue to pharmacologically target aberrant MAPK signaling required for malignant transformation (Fig. 3*D*).

ANOVA followed by a Tukey's multi-comparisons test. ***p = 0.0003, **p = 0.0028. CCS, Cu chaperone for superoxide dismutase; Cu, copper; ICP-MS, inductively-coupled plasma mass spectrometry; SPR, surface plasmon resonance.

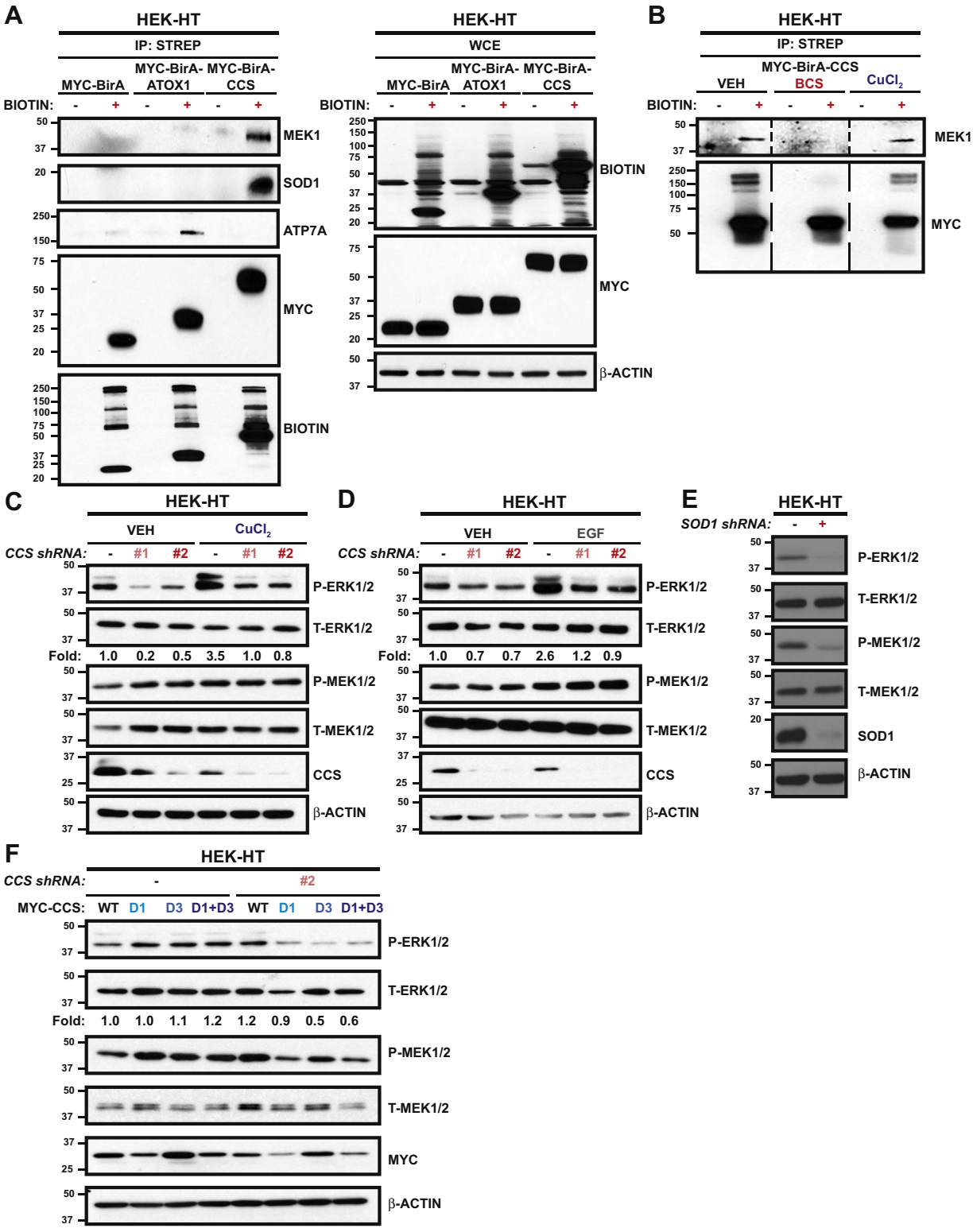

Figure 2. CCS is the necessary Cu chaperone for MEK1. *A*, immunoblot detection of biotinylated MEK1, ATP7A, SOD1, MYC-BirA, MYC-BirA-ATOX1, or MYC-BirA-CCS from strepavadin pulldowns and whole cell extracts from HEK-HT cells stably expressing *MYC-BirA*, *MYC-BirA-ATOX1*, or *MYC-BirA-CCS* treated with media with (+) or without (–) biotin for 48 h. n = 2 biologically independent experiments. *B*, immunoblot detection of biotinylated MEK1 or MYC-BirA-CCS from strepavadin pulldowns from HEK-HT cells stably expressing *MYC-BirA-CCS* treated with media with (+) or without (–) biotin for 48 h in the presence of vehicle, 500 μM bathocuproinedisulfonic acid (BCS), or 1 μM $CuCl_2$. n = 2 biologically independent experiments. *C* and *D*, immunoblot detection of phosphorylated (P)-ERK1/2, total (T)-ERK1/2, P-MEK1/2, T-MEK1/2, CCS, or β-ACTIN from HEK-HT cells stably expressing doxycycline inducible *shRNA* against control (–) or *CCS* (*#1 or #2*) treated with doxycycline for 24 h followed by (*B*), vehicle (VEH) or 1 μM $CuCl_2$ for 20 min or (*C*), VEH or 0.1 ng/ml EGF for 15 min. Quantification: Fold change P-ERK1/2/T-ERK1/2 normalized to control, VEH. n = 3 biologically independent experiments. *E*, immunoblot detection of P-ERK1/2, T-ERK1/2, P-MEK1/2, T-MEK1/2, SOD1, or β-ACTIN from HEK-HT cells stably expressing doxycycline inducible *shRNA* against control (–) or *SOD1* (+) treated with doxycycline for 48 h n = 2 biologically independent experiments. *F*, immunoblot detection of P-ERK1/2, T-ERK1/2, P-MEK1/2, T-MEK1/2, MYC, or

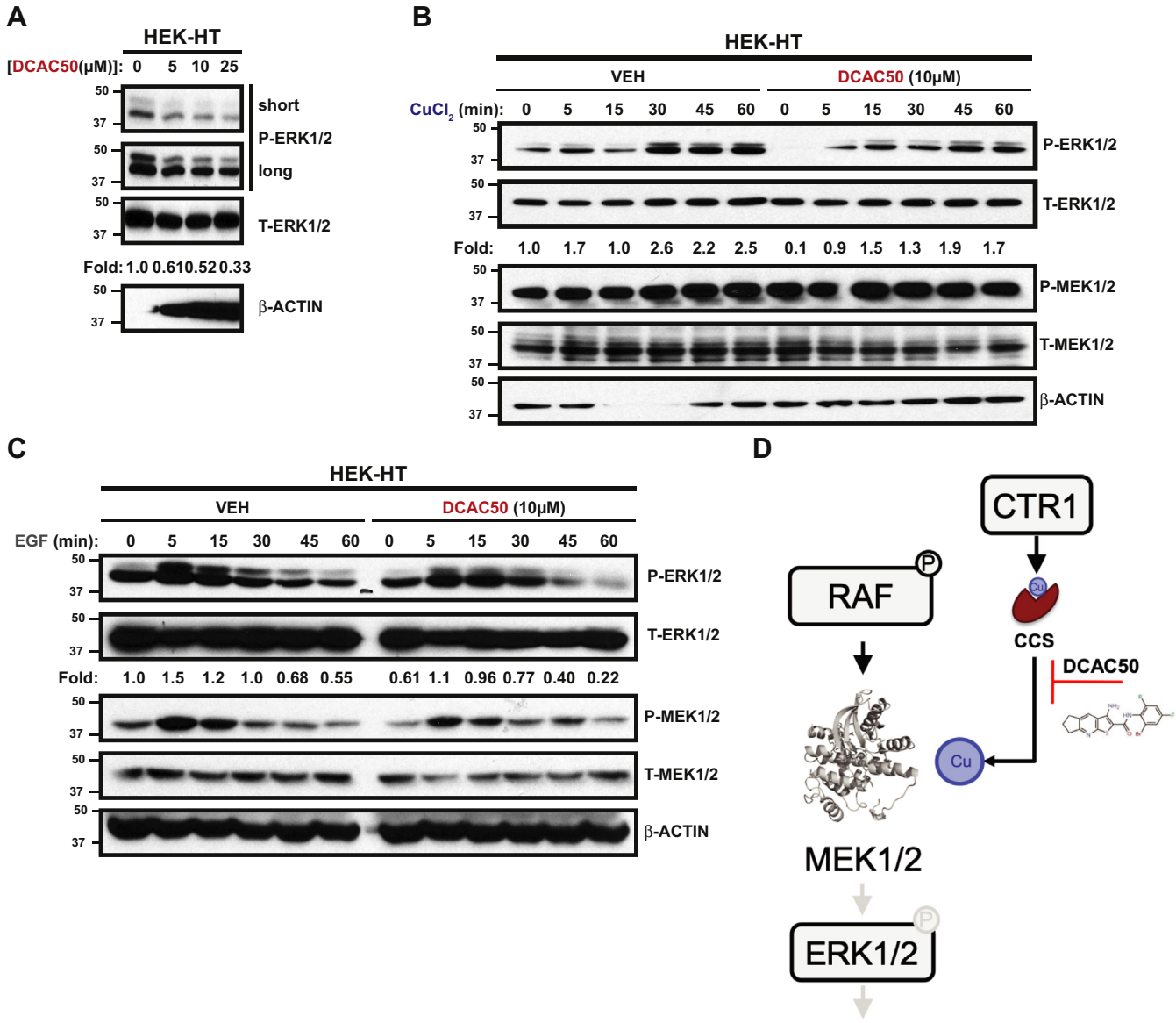

Figure 3. Treatment with small molecular inhibitor of CCS blunts MAPK pathway activation at the level of MEK1/2. *A*, immunoblot detection of phosphorylated (P)-ERK1/2, total (T)-ERK1/2, or β-ACTIN from HEK-HT cells treated with vehicle (0) or increasing concentrations of DCAC50 for 24 h. Quantification: Fold change P-ERK1/2/T-ERK1/2 normalized to control, VEH. n = 3 biologically independent experiments. *B* and *C*, immunoblot detection of P-ERK1/2, T-ERK1/2, P-MEK1/2, T-MEK1/2, or β-ACTIN from HEK-HT cells treated with vehicle (–) or 10 μM DCAC50 for 24 h followed stimulation with (*B*), 1 μM $CuCl_2$ or (*C*), 0.1 ng/ml EGF for indicated time. Quantification: Fold change P-ERK1/2/T-ERK1/2 normalized to control, VEH. n = 3 biologically independent experiments. *D*, model of CCS-mediated Cu activation of MEK1/2. CCS, Cu chaperone for superoxide dismutase; Cu, copper; EGF, epidermal growth factor; MAPK, mitogen-associated protein kinase; VEH, vehicle.

Discussion

Our previous discovery that Cu selectively regulates the canonical MAPK pathway at the level of the MEK1/2 kinases, in both *Drosophila* and mammalian cell settings, suggests that there is an evolutionarily conserved pressure for this integration (12). Further, it established a critical mechanistic function for Cu as an intracellular mediator of signaling, which was previously reserved for redox-inactive metals like Zn^{2+}, K^+, Na^+, and Ca^{2+} that have well appreciated roles in cell signaling (6). However, the cellular delivery mechanism of Cu to the dual specificity protein kinases MEK1/2 remained to be elucidated.

In support of the hypothesis that kinases within complex protein modules may directly respond to and/or sense metals like Cu, we found that short exposure to $CuCl_2$ was sufficient to robustly increase ERK1/2 phosphorylation (Figs. 2 and 3).

β-ACTIN from HEK-HT cells stably expressing doxycycline inducible *shRNA* against control (–) or *CCS* (*#2*) reconstituted with *MYC-CCS*^{WT}(WT), *MYC-CCS Domain 1 Mutant* (D1), *MYC-CCS Domain 3 Mutant* (D3), or *MYC-CCS Domain 1 + 3 Mutant* (D1+D3) treated with doxycycline for 24 h. Quantification: Fold change P-ERK1/2/T-ERK1/2 normalized to control, VEH. n = 3 biologically independent experiments. CCS, Cu chaperone for superoxide dismutase; Cu, copper; EGF, epidermal growth factor.

This observation indicates that MEK1/2 are not fully Cu bound in cells and are thus primed to rapidly respond to fluctuations in intracellular Cu levels. The cellular contexts in which labile Cu pools are liberated are under active investigation. Two recent reports provide evidence of this phenomena in which depletion of the intracellular glutathione pools (34) or amino acid deprivation (35) were sufficient to elevate Cu(I) levels. Further, both basal and growth factor stimulated MAPK signaling were diminished when point mutants of the Cu coordinating ligands were introduced, which suggests that Cu is a hardwired component of the pathway that is necessary for the other inputs.

To balance cellular toxicity from free Cu ions with metalation of cuproenzymes, the evolutionarily conserved Cu chaperones promote Cu distribution. Here, we show that the Cu chaperone for superoxide dismutase CCS transiently binds to and facilitates Cu loading into MEK1 and in turn increases MEK1/2 kinase activity (Fig. 1). In agreement with a whole genome RNAi screen in *Drosophila* S2 cells aimed at identifying modulators of MAPK signaling (36), the knockdown of *CCS* reduced ERK1/2 phosphorylation (Fig. 2). An intricate molecular mechanism requiring three distinct domains of CCS is required for SOD1 maturation and activation (27, 31, 32). Interestingly, D3 of CCS, which helps with Cu transfer into the SOD1 active site and generates a disulfide bond in SOD1 (27, 31, 32), was also necessary for robust MEK1/2 activation (Fig. 2). This finding suggests that the aforementioned Cu-mediated MEK1 disulfide formation may be installed by CCS in mammalian cells and mechanistically underlie MEK1 activation by Cu. Interestingly, *in vitro* experiments adding $CuCl_2$ to purified MEK1 protein resulted in inhibition, not activation, of the enzyme (data not shown), suggesting that Cu loading by CCS is required for activation, potentially to avoid Cu binding to other sites that might inhibit MEK1 activity or to facilitate complete maturation of the Cu bound state. However, the structural and molecular features of MEK1/2 that facilitate a specific interaction with CCS remain elusive. Notable alignment of either structure of sequence of CCS or SOD1 with MEK1 fails to provide an obvious explanation for the recognition of MEK1 by CCS. These preliminary analyses indicate that the similarity between CCS, SOD1, and MEK1 is weak but given the potential of targeting the structural CCS-MEK1 interface with small molecules, this line of investigation warrants future exploration. This result further supports the importance of CCS in controlling MEK1 activation *via* Cu.

Finally, pharmacologic targeting of CCS with the small molecule inhibitor DCAC50 (33) blunted both basal and stimulated activation of MEK1/2 (Fig. 3). Our previous work demonstrated that knockout of *ATOX1* in human BRAF mutation positive melanoma cells also decreased MAPK signaling (37). Although DCAC50 targets both CCS and ATOX1, exogenous $CuCl_2$ was sufficient to rescue P-ERK1/2, indicating that ATOX1 impacts MAPK pathway activation indirectly of facilitating Cu binding of MEK1/2. The vital importance of intricate mechanisms to dynamically regulate MAPK signaling output is underscored by its dysregulation in approximately 85% of the human cancers (21, 22). Although targeting the protein kinase catalytic activity of MEK1/2 is approved in the setting of $BRAF^{V600E}$ metastatic melanoma (22, 38) and is under investigation in several other cancers, resistance mechanisms limited clinical durability. Therefore, our structural and molecular studies provide a framework for the development of MEK1/2 inhibitors that exploit its Cu dependence by targeting the binding interface or intracellular delivery components.

Experimental procedures

Cell lines

HEK-HT cells were previously described (39) and provided by C.M. Counter (Duke University). The HEK-HT cells were maintained in the Dulbecco's Modified Eagle Media (DMEM, Gibco) supplemented with 10% v/v fetal bovine serum (FBS, GE Lifesciences) and 1% penicillin-streptomycin (P/S, Gibco). The HEK-HT cells were stably infected with lentiviruses derived from the pSMARTvector inducible lentiviral shRNA plasmids (Dharmacon, see Plasmids below) or retroviruses derived from the pWZL retroviral plasmid (see Plasmids below) described below using established methods.

Plasmids

pGEX4T3-HA-$ERK2^{K54R}$ (Addgene plasmid #53170) (24), pET3A-T7-HIS-ATOX1 (40), pWZLblasti-HA-$MEK1^{WT}$ (Addgene plasmid #53161) (24), and pET15B-HIS-PARVALBUMIN (41) were previously described. pETDUET-6XHIS-TEV-ATOX1 and pBABEpuro-MYC-BioID2-ATOX1 were created by PCR subcloning ATOX1 from pCDNA-ATOX1 (33) with primers for the pETDUET plasmid containing an N-terminal, TEV protease cleavable 6XHIS-tag or the pBABEpuro-MYC-BioID2 (Addgene #80900) (28) plasmid containing an N-terminal myc tag in frame with mutant BirA (R118G). pETDUET-6XHIS-TEV-CCS, pBABEpuro-MYC-BioID2-CCS, and pWZLblasti-MYC-CCS^{WT} were created by PCR subcloning CCS from pCDNA-CCS (33) with primers for the pETDUET plasmid containing an N-terminal, TEV protease cleavable 6XHIS-tag, for the pBABEpuro-MYC-BioID2 plasmid containing an N-terminal MYC-tag in frame with mutant BirA (R118G), or with primers including an N-terminal MYC-tag for the pWZLblasti plasmid. pKA8H-CCS was created by PCR subcloning CCS with primers for the pKA8H plasmid containing an N-terminal, TEV protease cleavable 8XHIS-tag. pWZLblasti-MYC-$CCS^{D1(C22A/C25A)}$, -$CCS^{D3(C244A/C246A)}$, and -$CCS^{D1+D3(C22A/C25A/C244A/C246A)}$ were created by introducing mutations corresponding to the indicated amino acid changes by site-directed mutagenesis into CCS^{WT} from the pWZLblasti-MYC-CCS^{WT} plasmid. pSMARTvector inducible lentiviral shRNA plasmids were purchased from Dharmacon to express nontargeted control, human CCS target sequence #1 5′-GGGCAGGCAAAGTCCCTCT, and human CCS target sequence #2 5′- AGTGGAAAGTGCTCGCCCT. GFP and shRNA expression was induced by adding 2 μg/ml doxycycline hydrochloride (Fisher Scientific, AAJ67043AE) to DMEM supplemented with 10% fetal bovine serum and 1% penicillin-streptomycin.

Protein expression and purification

Proteins used for in vitro *kinase assays*

GST-ERK2^{K54R}—GST-ERK2^{K54R} was expressed in BL21 (DE3) RIL cells in TB at 37 °C until reaching an A_{600} of 0.700 and then induced with 1 mM IPTG overnight at 17 °C. The cells were then spun down the next day and lysed in lysis buffer 1 (25 mM Tris pH 7.5, 500 mM NaCl, and 5 mM β-mercaptoethanol [BME]) treated with 1 mM PMSF and DNAseI. The lysate was then spun down at 19,000 rpm for 40 min, and the supernatant was added to 10 ml of glutathione agarose resin (Pierce, 16102BID) previously washed with lysis buffer 1 and left to incubate at 4 °C for 2 h. The supernatant was eluted *via* gravity column, and the resin was then washed with 1 L of lysis buffer 1. The protein was then eluted with lysis buffer 1 supplemented with 20 mM glutathione (Sigma Aldrich # G4521), and the elution fractions were pooled together and dialyzed into dialysis buffer 1 (25 mM Tris pH 7.5, 150 mM NaCl, and 5 mM BME). The protein was then concentrated and applied to a Superdex S200 10/300 gel filtration column in a final buffer of 25 mM Tris pH 7.5, 150 mM NaCl, and 5 mM BME.The protein was concentrated to 2.4 mg/ml (35 μM), flash frozen in liquid nitrogen, and stored in −80 °C freezer for future use.

6XHIS-ATOX1—6XHIS-ATOX1 was expressed in BL21 (DE3) RIL cells in LB (Millipore) at 37 °C until reaching an A_{600} of 0.700 and then induced with 1 mM IPTG overnight at 17 °C. The cells were then spun down the next day and lysed in lysis buffer 1 (25 mM Tris pH 7.5, 500 mM NaCl, and 5 mM BME) treated with 1 mM PMSF and DNAseI. The lysate was then spun down at 19,000 rpm for 40 min, and the supernatant was added to 10 ml of HisPur nickel-nitrilotriacetic acid (Ni-NTA) resin previously washed with lysis buffer 1 and left to incubate at 4 °C for 1 h. The supernatant was eluted *via* gravity column, and the resin was then washed with 1 L of lysis buffer 1 treated with 20 mM imidazole. The protein was then eluted with lysis buffer 1 supplemented with 300 mM imidazole, and the elution fractions were pooled together and treated with TEV protease overnight while dialyzing into dialysis buffer 1 (25 mM Tris pH 7.5, 20 mM NaCl, 5 mM BME). The eluent is then applied to a HiTrap Q HP anion exchange 5 ml column and eluted over a gradient of 20 column volumes ranging from 0% to 100% of buffer B (25 mM Tris pH 7.5, 1 M NaCl, and 5 mM BME). The peak fractions were run on an SDS-PAGE gel, pooled, concentrated, and applied to 10 ml of fresh Ni-NTA resin washed with reverse nickel buffer 1 (25 mM Tris pH 7.5, 250 mM NaCl, 20 mM imidazole, and 5 mM BME). The protein was allowed to pass over the nickel resin three times and then washed extensively with reverse nickel buffer 1 until no more protein was washed off the resin as monitored by Bradford Reagent. The protein was then concentrated and added to a Superdex S200 10/300 gel filtration column in a final buffer of 20 mM Hepes pH 7.0, 150 mM NaCl, and 5 mM BME. The protein was concentrated to ∼6 mg/ml (∼650 μM) and dialyzed into dialysis buffer 2 (20 mM Hepes pH 7.0, 150 mM NaCl, and 3.25 mM DTT) overnight. The next morning, 1M $CuCl_2$ was added to 650 μM of ATOX1 to a final concentration of 585 μM of $CuCl_2$ and mixed until dissolved. The protein loaded with Cu was then flash frozen in liquid nitrogen and stored in −80 °C freezer for future use.

6XHIS-CCS—6XHIS-CCS was expressed in BL21 (DE3) RIL cells in LB at 37 °C until reaching an A_{600} of 0.700 and then induced with 1 mM IPTG overnight at 17 °C. The cells were then spun down the next day and lysed in lysis buffer 1 (25 mM Tris pH 7.5, 500 mM NaCl, and 5 mM BME) treated with 1 mM PMSF and DNAseI. The lysate was then spun down at 19,000 rpm for 40 min, and the supernatant was added to 10 ml of HisPur Ni-NTA resin previously washed with lysis buffer 1 and left to incubate at 4 °C for 1 h. The supernatant was eluted *via* gravity column, and the resin was then washed with 1 L of lysis buffer 1 treated with 20 mM imidazole. The protein was then eluted with lysis buffer 1 supplemented with 300 mM imidazole, and the elution fractions were pooled together and treated with TEV protease overnight while dialyzing into dialysis buffer 1 (25 mM Tris pH 7.5, 20 mM NaCl, and 5 mM BME). The eluent is then applied to a HiTrap Q HP anion exchange 5 ml column and eluted over a gradient of 20 column volumes ranging from 0% to 100% of buffer B (25 mM Tris pH 7.5, 1 M NaCl, and 5 mM BME). The peak fractions were run on an SDS-PAGE gel, pooled, concentrated, and applied to 10 ml of fresh Ni-NTA resin washed with reverse nickel buffer 1 (25 mM Tris pH 7.5, 250 mM NaCl, 20 mM imidazole, and 5 mM BME). The protein was allowed to pass over the nickel resin three times and then washed extensively with reverse nickel buffer 1 until no more protein was washed off the resin as monitored by Bradford Reagent. The protein was then concentrated and added to a Superdex S200 10/300 gel filtration column in a final buffer of 20 mM Hepes pH 7.0, 150 mM NaCl, and 5 mM BME. The protein was concentrated to ∼20 mg/ml (∼650 μM) and dialyzed into dialysis buffer 2 (20 mM Hepes pH 7.0, 150 mM NaCl, and 3.25 mM DTT) overnight. The next morning, 1M $CuCl_2$ was added to 650 μM of CCS to a final concentration of 585 μM of $CuCl_2$ and mixed until dissolved. The protein loaded with Cu was then flash frozen in liquid nitrogen and stored in −80 °C freezer for future use.

Proteins used for surface plasmon resonance

T7-HIS-ATOX1—T7-HIS-ATOX1 was expressed in BL21 (DE3) cells in LB with carbenicillin (100 μg/ml, Sigma Aldrich) and when reached the exponential growth, IPTG (Sigma Aldrich) was added. Protease inhibition cocktail (Roche) was added to prevent protein degradation and the cells were lysed by sonication. Nucleic acids digestion was performed with universal nuclease (Pierce). The proteins were then purified using an ÄKTA Purifier (GE Healthcare). First, the protein was purified with a HisTrap FF Ni-NTA column (GE Healthcare), using a gradient of imidazole (5 mM–1 M). Second, further purification was done with a

Q Sepharose Fast Flow column (GE Healthcare) and a gradient of NaCl (50 mM–500 mM). Finally, the last purification step was size exclusion using a HiLoad 16/600 Superdex 75 pg column (GE Healthcare). The protein was concentrated with a 3 kDa Amicon Ultra Centrifugal filter (Sigma-Aldrich).

HIS-CCS—HIS-CCS was purchased from Protein Expression Platform at Umeå University.

HIS-PARVALBUMIN—HIS-PARVALBUMIN purification was previously described (41).

Proteins used for electrophoretic mobility shift assays (EMSAs) and size exclusion chromatography (SEC)

8XHIS-CCS *and* 6XHIS-MEK1—8XHIS-CCS and 6XHIS-MEK1 proteins were expressed in BL21 (DE3) pLysS cells in LB media at 37 °C until reaching an A_{600} of 0.6 to 0.8 and then induced with 1 mM IPTG for an additional 4 h before being harvested. 8XHIS-CCS protein was purified using a HisTrap HP Ni affinity column (Amersham Biosciences) using buffer A (20 mM Tris, pH 8, 300 mM NaCl, and 2 mM DTT) and buffer B (20 mM Tris, pH 8, 300 mM NaCl, 2 mM TCEP, and 1M imidazole). The column was washed with 2% buffer B for 10 bed volume and CCS eluted with a gradient from 2% to 100% in 80 ml. The 8XHIS-tag was removed from the proteins using TEV protease produced in-house and engineered to contain its own noncleavable 8XHIS-tag. After digestion overnight at room temperature, the cleaved HIS-tag and TEV protease were removed from the sample by another pass through the nickel column. The 6XHIS-MEK1 proteins were purified using buffer A (50 mM Hepes, pH 7.5, 150 mM NaCl, and 1 mM TCEP) and buffer B (50 mM Hepes, pH 7.5, 150 mM NaCl, 1 mM TCEP, and 1 M imidazole), as described above.

Surface plasmon resonance

The interaction between MEK1 and HIS-ATOX1 or HIS-CCS was examined using a Biacore X100 surface plasmon resonance instrument (GE Healthcare). MEK1 was covalently coupled to a CM5 chip (GE Healthcare) using the amine coupling kit according to manufacturer's instructions (GE healthcare). Briefly, the surface was activated using 0.05 M N-hydroxysuccinimide and 0.4 M 1-ethyl-3-(-3-dimethylaminopropyl) carbodiimide hydrochloride before the injection of MEK1 (20 μg/ml in sodium acetate buffer, pH 4.5) until 2000 RU (∼2 ng/mm2) was reached and, finally, 1M ethanolamine was injected for deactivation of the surface. The interaction was measured at 25 °C in HBS-P+ running buffer containing 10 mM Hepes, 150 mM NaCl, and 0.001% P20 detergent at pH 7.4 (GE Healthcare). Increasing concentrations (2x increase for every injection) of HIS-ATOX1 or HIS-CCS were flown over the surface in a single-cycle sequence without regeneration steps between injections. At the end of the cycle, regeneration was done by injection of 50 mM NaOH (GE Healthcare). The samples of HIS-ATOX1 and HIS-CCS were prepared with DTT (Sigma Aldrich) with a molar ratio of 5:1 (DTT:protein) and for experiments conducted with Cu ($CuCl_2$ from Sigma Aldrich), with a molar ratio of 0.9:1 for $CuCl_2$:protein. The dissociation constant, K_d, was determined with the BIAevaluation software using the 1:1 binding model. To confirm that the HIS-tag was not significant for the binding, an equivalent experiment using HIS-PARVALBUMIN was performed.

Electrophoretic mobility shift assays

Metal content of proteins was determined by ICP-MS before experimental set-up. Binding assays were performed in triplicate at pH 7.5 in 50 mM Hepes, 150 mM NaCl, and 1 mM TCEP. The assays were conducted using apo-CCS and Cu(I)-CCS with CCS in excess and MEK1 constant. Experimental concentrations were chosen based on the affinity determined previously by SPR at 8 μM. Protein reactions were allowed to incubate 20 min at room temperature before native gel analysis. 10% native gels were loaded with 10ul of each reaction with 2ul of 50% glycerol added. The gels were run at 150 V for 60 min and then stained with Coomassie blue for 20 min. The gels were de-stained overnight with agitation and visualized using the ChemiDoc MP system (BioRad).

In vitro *kinase assay*

The activity and activation of $MEK1^{WT}$ by Cu chaperones ATOX1 or CCS were assessed using an ELISA assay adapted from a previously established assay (42). Briefly, GST-$ERK2^{K54R}$ fusion protein was diluted to a final concentration of 5.33 μM in Tris-buffered saline treated with 0.05% Tween-20 (TBST) and added to a glutathione-coated 96 well plate (Pierce, #15240) and incubated at room temperature for 1 h with shaking. Purified and untagged full-length $MEK1^{WT}$ and mutants were diluted to 400 nM concentrations in kinase buffer 1 (50 mM Hepes pH 7.0 and 50 mM NaCl), and 3 μl of various concentrations of CCS were added to 100 μl of diluted MEK in a 96-well "V" bottom plate (Corning, #2897) to final concentrations ranging from 1.25 μM to 10 μM. The MEK1/ATOX1 or MEK1/CCS mixture was then incubated for 1 h at room temperature. The glutathione-coated plates were then washed extensively with TBST, and 50 μl of the MEK1 ATOX or MEK1/CCS mixture was added to the $ERK2^{K54R}$-bound plates along with 50 μl of 200 μM ATP in ATP dilution buffer (50 mM Hepes pH 7.0, 200 mM NaCl, and 20 mM $MgCl_2$) bring the final reaction concentrations to 200 nM MEK and 100 μM ATP. The plate was then mixed at room temperature for 5 min and then left to incubate in a 37 °C incubator for 30 min. The reaction was then washed from the plate, and the plate was extensively washed with TBST to quench the reaction. A 1:5000 dilution of rabbit anti-phospho(Thr202/Tyr204)-ERK1/2 (Cell Signaling Technology (CST), 9101) in TBST treated with 0.5% BSA was added to the plate and incubated for 1 h at room temperature with shaking. The plate was then treated to multiple TBST washes and then incubated with a 1:5000 dilution of secondary antibody (goat anti-rabbit IgG (H + L)-HRP (BioRad)) in TBST treated with 0.5% BSA for 1 h with shaking at room temperature. The plate was again

washed with multiple TBST washes, and Supersignal ELISA Pico Chemiluminescent Substrate (Pierce, #37069) was added. The plate was read on a Promega GloMAX 96 Microplate Luminometer. Statistical analysis of P-ERK2 luminescence units was analyzed using a one-way ANOVA followed by a Dunnett's multi-comparisons test or a two-way ANOVA followed by a Tukey's multi-comparisons test in Prism 7 (GraphPad).

Immunoblot analysis

The HEK-HT parental cells or those stably expressing pSMARTvector constructs were treated as indicated and washed with cold PBS and lysed with cold radioimmunoprecipitation assay buffer containing 1X EDTA-free Halt protease and phosphatase inhibitor cocktail halt protease and phosphatase inhibitors (Thermo Scientific). Protein concentration was determined by BCA Protein Assay (Pierce) using BSA as a standard. Equal amount of lysates were resolved by SDS-PAGE using standard techniques, and protein was detected with the following primary antibodies: mouse anti-ATP7A (1:1000; 376467, Santa Cruz), mouse anti-β-ACTIN (1:10,000; 3700, Cell Signaling), rabbit anti-biotin (1:1000; 5597, Cell Signaling), mouse anti-CCS (1:1000; 55561, Santa Cruz), rabbit anti-phospho(Thr202/Tyr204)-ERK1/2 (1:1000; 9101, Cell Signaling), mouse anti-ERK1/2 (1:1000; 9107, Cell Signaling), rabbit anti-phospho(Ser217/221)-MEK1/2 (1:1000; 9154S, Cell Signaling), mouse anti-MEK1/2 (1:1000; 4694S, Cell Signaling), mouse anti-MEK1 (1:1000; 2352, Cell Signaling), mouse anti-MYC (1:1000; 227S, Cell Signaling), and mouse anti-SOD1 (1:1000; MA1-105, ThermoFisher Scientific) followed by detection with one of the horseradish peroxidase conjugated secondary antibodies: goat anti-rabbit IgG (1:2000; 7074, Cell Signaling) or goat anti-mouse (1:2000; 7076, Cell Signaling) using SignalFire (Cell Signaling) or SignalFire Elite ECL (Cell Signaling) detection reagents. The fold change in the ratio of phosphorylated protein to total protein was measured in Image Studio Lite (LI-COR Biosciences) software by boxing each band using the rectangular selection tool and calculating the signal of the band in pixels. The signal of the phosphorylated protein band in pixels was normalized to the signal of the total protein band in pixels. The average fold change is shown in figures. For BirA proximity-dependent biotin labeling studies, the HEK-HT cells stably expressing MYC-BirA, MYC-BirA-ATOX1, or MYC-BirA-CCS were treated with or without biotin for 24 h, as previously described, and the biotinylated proteins were pulled down with Dynabeads MyOne Streptavidin C1 (Life Technologies, #65002), as previously described.

Size exclusion chromatography

SEC of MEK1 and CCS were conducted to determine elution volume using Superdex 75 Increase 10/300 Gl (GE Healthcare). Cu(I)-CCS was mixed in equal ratio with MEK1 in the presence or absence of 5:1 M ratio BCS(Sigma Aldrich # 146625) to protein and the mixture subjected to SEC. The flow rate of each purification was 0.5 ml/min using 50 mM Hepes, pH 7.5, 150 mM NaCl, and 1 mM TCEP buffer. ICP-MS determined the metal content of proteins before experimental set-up.

SOD1 activity assays

SOD1 activity was visualized by an *in situ* gel assay through staining with nitro blue tetrazolium, as previously described (29, 43).

Data availability

All data are contained within the article. The raw data for these studies is available from the senior author at bradyd@pennmedicine.upenn.edu.

Supporting information—This article contains supporting information.

Acknowledgments—We thank C. M. Counter (Duke University), J. Chen (Emory University), and P. Hart (University of Texas Health Science Center at San Antonio) for reagents; L. A. Brady, L. Busino, and E. S. Witze for technical support, discussions, and/or review of the manuscript; and D. Sneddon for administrative support.

Author contributions—M. G., R. M., and D. C. B. conceptualization; M. G., G. J. B., Y.-J. K., S. B., M. M. D., S. V., T. T., N. A. S., K. B. A., P. W.-S., D. D. W., R. M., and D. C. B. data curation; M. G., G. J. B., Y.-J. K., S. B., M. M. D., S. V., T. T., N. A. S., K. B. A., R. M., and D. C. B. formal analysis; P. W.-S., D. D. W., R. M., and D. C. B. supervision; M. G., G. J. B., Y.-J. K., S. B., M. M. D., S. V., T. T., N. A. S., and D. C. B. validation; M. G., G. J. B., Y.-J. K., S. B., M. M. D., S. V., T. T., N. A. S., K. B. A., N. J. B., G. M. B., P. W.-S., D. D. W., and D. C. B. investigation; M. G., G. J. B., Y.-J. K., S. B., M. M. D., S. V., T. T., N. A. S., and D. C. B. visualization; M. G., G. J. B., Y.-J. K., S. B., M. M. D., S. V., T. T., N. A. S., K. B. A., N. J. B., G. M. B., P. W.-S., D. D. W., R. M., and D. C. B. methodology; M. G., G. J. B., Y.-J. K., S. B., M. M. D., S. V., T. T., N. J. B., G. M. B., P. W.-S., D. D. W., R. M., and D. C. B. writing–original draft; M. G., M. M. D., and D. C. B. project administration; M. G., G. J. B., Y.-J. K., S. B., M. M. D., S. V., T. T., N. A. S., K. B. A., N. J. B., G. M. B., P. W.-S., D. D. W., R. M., and D. C. B. writing–review and editing; G. M. B., P. W.-S., D. D. W., and R. M. resources.

Funding and additional information—This work was supported by NIH grants GM124749 (D. C. B.), CA243294 (T. T.), GM123725 (N. J. B.), and GM136239 (N. J. B.), Swedish Research Council Grant 2015-03881 (P. W.-S.), Knut and Alice Wallenberg Foundation Scholar Grant (P. W.-S.), and Pew Scholars Program in Biomedical Science Award #50359 (D. C. B.). The content is solely the responsibility of the authors and does not necessarily represent the official views of the National Institutes of Health.

Conflict of interest—D. C. B. holds ownership in Merlon Inc. D. C. B. is an inventor on the patent application 20150017261 entitled "Methods of treating and preventing cancer by disrupting the binding of copper in the MAP kinase pathway". All other authors declare that they have no conflicts of interest with the contents of this article.

Abbreviations—The abbreviations used are: BCS, bathocuproinedisulfonic; BioID, biotin identification; BME, β-mercaptoethanol; BSA, bovine serum albumin; CCS, Cu chaperone for superoxide dismutase; Cu, copper; ICP-MS, inductively-coupled

plasma mass spectrometry; MAPK, mitogen-associated protein kinase; Ni-NTA, nickel-nitrilotriacetic acid; SPR, surface plasmon resonance; SEC, size-exclusion chromatography; TBST, tris-buffered saline with Tween-20.

References

1. Kolch, W., Halasz, M., Granovskaya, M., and Kholodenko, B. N. (2015) The dynamic control of signal transduction networks in cancer cells. *Nat. Rev. Cancer* **15**, 515–527
2. Efeyan, A., Comb, W. C., and Sabatini, D. M. (2015) Nutrient-sensing mechanisms and pathways. *Nature* **517**, 302–310
3. Manning, G., Plowman, G. D., Hunter, T., and Sudarsanam, S. (2002) Evolution of protein kinase signaling from yeast to man. *Trends Biochem. Sci.* **27**, 514–520
4. Thiele, D. J., and Gitlin, J. D. (2008) Assembling the pieces. *Nat. Chem. Biol.* **4**, 145–147
5. Kim, B. E., Nevitt, T., and Thiele, D. J. (2008) Mechanisms for copper acquisition, distribution and regulation. *Nat. Chem. Biol.* **4**, 176–185
6. Chang, C. J. (2015) Searching for harmony in transition-metal signaling. *Nat. Chem. Biol.* **11**, 744–747
7. Ala, A., Walker, A. P., Ashkan, K., Dooley, J. S., and Schilsky, M. L. (2007) Wilson's disease. *Lancet* **369**, 397–408
8. Kaler, S. G. (2014) Translational research investigations on ATP7A: An important human copper ATPase. *Ann. N. Y. Acad. Sci.* **1314**, 64–68
9. Mercer, J. F., Livingston, J., Hall, B., Paynter, J. A., Begy, C., Chandrasekharappa, S., Lockhart, P., Grimes, A., Bhave, M., Siemieniak, D., and Glover, T. W. (1993) Isolation of a partial candidate gene for Menkes disease by positional cloning. *Nat. Genet.* **3**, 20–25
10. Yamaguchi, Y., Heiny, M. E., and Gitlin, J. D. (1993) Isolation and characterization of a human liver cDNA as a candidate gene for Wilson disease. *Biochem. Biophys. Res. Commun.* **197**, 271–277
11. Turski, M. L., and Thiele, D. J. (2009) New roles for copper metabolism in cell proliferation, signaling, and disease. *J. Biol. Chem.* **284**, 717–721
12. Turski, M. L., Brady, D. C., Kim, H. J., Kim, B. E., Nose, Y., Counter, C. M., Winge, D. R., and Thiele, D. J. (2012) A novel role for copper in Ras/mitogen-activated protein kinase signaling. *Mol. Cell. Biol.* **32**, 1284–1295
13. Lee, J., Petris, M. J., and Thiele, D. J. (2002) Characterization of mouse embryonic cells deficient in the ctr1 high affinity copper transporter. Identification of a Ctr1-independent copper transport system. *J. Biol. Chem.* **277**, 40253–40259
14. Turski, M. L., and Thiele, D. J. (2007) Drosophila Ctr1A functions as a copper transporter essential for development. *J. Biol. Chem.* **282**, 24017–24026
15. Dancis, A., Yuan, D. S., Haile, D., Askwith, C., Eide, D., Moehle, C., Kaplan, J., and Klausner, R. D. (1994) Molecular characterization of a copper transport protein in S. cerevisiae: An unexpected role for copper in iron transport. *Cell* **76**, 393–402
16. Morrison, D. K. (2012) MAP kinase pathways. *Cold Spring Harb. Perspect. Biol.* **4**, a011254
17. Cobb, M. H. (1999) MAP kinase pathways. *Prog. Biophys. Mol. Biol.* **71**, 479–500
18. Terrell, E. M., and Morrison, D. K. (2019) Ras-mediated activation of the Raf family kinases. *Cold Spring Harb. Perspect. Med.* **9**, a033746
19. Friedman, A., and Perrimon, N. (2006) High-throughput approaches to dissecting MAPK signaling pathways. *Methods* **40**, 262–271
20. Davies, H., Bignell, G. R., Cox, C., Stephens, P., Edkins, S., Clegg, S., Teague, J., Woffendin, H., Garnett, M. J., Bottomley, W., Davis, N., Dicks, E., Ewing, R., Floyd, Y., Gray, K., *et al.* (2002) Mutations of the BRAF gene in human cancer. *Nature* **417**, 949–954
21. Holderfield, M., Deuker, M. M., McCormick, F., and McMahon, M. (2014) Targeting RAF kinases for cancer therapy: BRAF-mutated melanoma and beyond. *Nat. Rev. Cancer* **14**, 455–467
22. Caunt, C. J., Sale, M. J., Smith, P. D., and Cook, S. J. (2015) MEK1 and MEK2 inhibitors and cancer therapy: The long and winding road. *Nat. Rev. Cancer* **15**, 577–592
23. Brady, D. C., Crowe, M. S., Greenberg, D. N., and Counter, C. M. (2017) Copper chelation inhibits BRAFV600E-driven melanomagenesis and counters resistance to BRAFV600E and MEK1/2 inhibitors. *Cancer Res.* **77**, 6240–6252
24. Brady, D. C., Crowe, M. S., Turski, M. L., Hobbs, G. A., Yao, X., Chaikuad, A., Knapp, S., Xiao, K., Campbell, S. L., Thiele, D. J., and Counter, C. M. (2014) Copper is required for oncogenic BRAF signalling and tumorigenesis. *Nature* **509**, 492–496
25. Kim, Y.-J., Tsang, T., Anderson, G. R., Posimo, J. M., and Brady, D. C. (2020) Inhibition of BCL2 family members increases the efficacy of copper chelation in BRAFV600E-driven melanoma. *Cancer Res.* **80**, 1387–1400
26. Xu, M., Casio, M., Range, D. E., Sosa, J. A., and Counter, C. M. (2018) Copper chelation as targeted therapy in a mouse model of oncogenic BRAF-driven papillary thyroid cancer. *Clin. Cancer Res.* **24**, 4271–4281
27. Robinson, N. J., and Winge, D. R. (2010) Copper metallochaperones. *Annu. Rev. Biochem.* **79**, 537–562
28. Kim, D. I., Jensen, S. C., Noble, K. A., Kc, B., Roux, K. H., Motamedchaboki, K., and Roux, K. J. (2016) An improved smaller biotin ligase for BioID proximity labeling. *MBoC* **27**, 1188–1196
29. Culotta, V. C., Klomp, L. W. J., Strain, J., Casareno, R. L. B., Krems, B., and Gitlin, J. D. (1997) The copper chaperone for superoxide dismutase. *J. Biol. Chem.* **272**, 23469–23472
30. Juarez, J. C., Manuia, M., Burnett, M. E., Betancourt, O., Boivin, B., Shaw, D. E., Tonks, N. K., Mazar, A. P., and Doñate, F. (2008) Superoxide dismutase 1 (SOD1) is essential for H2O2-mediated oxidation and inactivation of phosphatases in growth factor signaling. *Proc. Natl. Acad. Sci. U. S. A.* **105**, 7147–7152
31. Fetherolf, M. M., Boyd, S. D., Taylor, A. B., Kim, H. J., Wohlschlegel, J. A., Blackburn, N. J., Hart, P. J., Winge, D. R., and Winkler, D. D. (2017) Copper-zinc superoxide dismutase is activated through a sulfenic acid intermediate at a copper ion entry site. *J. Biol. Chem.* **292**, 12025–12040
32. Boyd, S. D., Calvo, J. S., Liu, L., Ullrich, M. S., Skopp, A., Meloni, G., and Winkler, D. D. (2019) The yeast copper chaperone for copper-zinc superoxide dismutase (CCS1) is a multifunctional chaperone promoting all levels of SOD1 maturation. *J. Biol. Chem.* **294**, 1956–1966
33. Wang, J., Luo, C., Shan, C., You, Q., Lu, J., Elf, S., Zhou, Y., Wen, Y., Vinkenborg, J. L., Fan, J., Kang, H., Lin, R., Han, D., Xie, Y., Karpus, J., *et al.* (2015) Inhibition of human copper trafficking by a small molecule significantly attenuates cancer cell proliferation. *Nat. Chem.* **7**, 968–979
34. Chung, C. Y.-S., Posimo, J. M., Lee, S., Tsang, T., Davis, J. M., Brady, D. C., and Chang, C. J. (2019) Activity-based ratiometric FRET probe reveals oncogene-driven changes in labile copper pools induced by altered glutathione metabolism. *Proc. Natl. Acad. Sci. U. S. A.* **116**, 18285–18294
35. Tsang, T., Posimo, J. M., Gudiel, A. A., Cicchini, M., Feldser, D. M., and Brady, D. C. (2020) Copper is an essential regulator of the autophagic kinases ULK1/2 to drive lung adenocarcinoma. *Nat. Cell Biol.* **22**, 412–424
36. Friedman, A., and Perrimon, N. (2006) A functional RNAi screen for regulators of receptor tyrosine kinase and ERK signalling. *Nature* **444**, 230–234
37. Kim, Y.-J., Bond, G. J., Tsang, T., Posimo, J. M., Busino, L., and Brady, D. C. (2019) Copper chaperone ATOX1 is required for MAPK signaling and growth in BRAF mutation-positive melanoma. *Metallomics* **11**, 1430–1440
38. Flaherty, K. T., Robert, C., Hersey, P., Nathan, P., Garbe, C., Milhem, M., Demidov, L. V., Hassel, J. C., Rutkowski, P., Mohr, P., Dummer, R., Trefzer, U., Larkin, J. M. G., Utikal, J., Dreno, B., *et al.* (2012) Improved survival with MEK inhibition in BRAF-mutated melanoma. *N. Engl. J. Med.* **367**, 107–114
39. Hahn, W. C., Counter, C. M., Lundberg, A. S., Beijersbergen, R. L., Brooks, M. W., and Weinberg, R. A. (1999) Creation of human tumour cells with defined genetic elements. *Nature* **400**, 464–468

40. Horvath, I., Blockhuys, S., Šulskis, D., Holgersson, S., Kumar, R., Burmann, B. M., and Wittung-Stafshede, P. (2019) Interaction between copper chaperone Atox1 and Parkinson's disease protein α-synuclein includes metal-binding sites and occurs in living cells. *ACS Chem. Neurosci.* **10**, 4659–4668
41. Werner, T., Kumar, R., Horvath, I., Scheers, N., and Wittung-Stafshede, P. (2018) Abundant fish protein inhibits α-synuclein amyloid formation. *Sci. Rep.* **8**, 5465
42. Grasso, M., Estrada, M. A., Ventocilla, C., Samanta, M., Maksimoska, J., Villanueva, J., Winkler, J. D., and Marmorstein, R. (2016) Chemically linked vemurafenib inhibitors promote an inactive BRAFV600E conformation. *ACS Chem. Biol.* **11**, 2876–2888
43. Schmidt, P. J., Rae, T. D., Pufahl, R. A., Hamma, T., Strain, J., O'Halloran, T. V., and Culotta, V. C. (1999) Multiple protein domains contribute to the action of the copper chaperone for superoxide dismutase. *J. Biol. Chem.* **274**, 23719–23725